國立臺灣大學工學院化學工程學系

碩士論文

Department of Chemical Engineering

College of Engineering

National Taiwan University

Master Thesis

在具有瞬間擴張之U型管道中的毛細現象

Imbibition Dynamics in U-groove Microchannel

with Sudden Enlargement

陳冠臨

Guan-Lin Chen

指導教授: 諶玉真 博士

Advisor: Yu-Jane Sheng, Ph.D.

中華民國 112 年 6 月

June, 2023

國立臺灣大學碩(博)士學位論文
口試委員會審定書

在具有瞬間擴張之U型管道中的毛細現象
Imbibition Dynamics in U-groove Microchannel
with Sudden Enlargement

本論文係陳冠臨君（　R10524046　）在國立臺灣大學化學工程學系、所完成之碩（博）士學位論文，於民國 112 年 06 月 15 日承下列考試委員審查通過及口試及格，特此證明

口試委員：

_____（簽名）

（指導教授）

系主任、所長 _____（簽名）

致謝

不知不覺我即將從國立台灣大學化學工程研究所碩士班畢業,攻讀碩士的這兩年來,除了日常修課與研究增進知識,日常生活中也發生了許多難以忘懷的回憶,我會謹記這些知識與回憶,帶著它們迎向下一階段的人生。

首先,我要對指導老師 諶玉真教授以及 曹恆光教授表示深深的感謝,兩位老師給予我研究上的指引,最終得以完成這篇研究。感謝 諶玉真教授在日常討論中,除了授予我研究知識外,當研究遇到瓶頸時,時常鼓勵我給予我信心,在課業上也時常關心我們的修課情況,使我能兼顧課業又能將研究做完善。也特別感謝 曹恆光教授對於本研究的指導,經過老師的嚴謹指導,使我在實驗研究設計、論點闡述與證明的部分有了更進一步的學習與認知,也增進了該領域的相關知識。也感謝兩位老師資助實驗室出遊,讓我們在研究之餘也能好好放鬆心情。

再來我想感謝在實驗室的夥伴們,包括千又、庭瑜、冠郁、明璋、昕緯、昱浩、心瑀、致融、斯楷、習鈞、雅雯以及慧新,不管是在實驗室出遊或是日常實驗室生活都讓我有不少美好回憶。感謝千又以及庭瑜平常和我討論課業以及研究,使我在研究所修課順利之外,在研究上也能互相關心彼此,促使彼此進步;感謝明璋學長與冠郁學姊,除了碩一進實驗室帶我認識研究領域與程式外,平時也時常關心我的實驗進展並給予我相關協助,使我研究更順利;感謝昱浩學長與心瑀學姊,細心教導我一些我不熟悉的知識與研究內容;感謝昕緯學長,平時和我聊遊戲,讓我在研究之餘也能好好放鬆;也感謝碩一的學弟妹們,協助處理研究外的事物,使我能專注於研究。感謝在實驗室的夥伴們,使我碩士生活得以圓滿。

最後,也要感謝口試委員 陳儀帆教授以及 黃俊仁教授協助我完善這份碩士論文。也要感謝我的父母給予我的支持與鼓勵,在當時大學推甄碩士班時也給予我建議,沒有父母的默默付出,就不會有現在的我;也感謝一起在台大化工所就讀的大學同學們,和你們一起討論課業與玩樂,讓我研讀碩士班能更順利。

摘要

本研究利用多體耗散粒子動力學模擬並探討在具有瞬間擴張且存在 Concus-Finn (CF) filamet 之矩形 U 型管道中的毛細現象。對於尾端開放之瞬間擴張管道,依據接觸角θ_y、與 CF filamet 有關之臨界角θ_f以及與主要流動有關之θ_c能分出四種流動類型。首先,在$\theta_y > \theta_f$ 和 $\theta_y > \theta_c$情況下,無邊角流動,且主要流動停止於小 U 形槽的末端; 其次,在$\theta_c > \theta_y > \theta_f$情況下,無邊角流動但主要流動存在;第三,在$\theta_f > \theta_y > \theta_c$情況下,邊角流動發生在大 U 形槽中但主要流動不存在;第四,在$\theta_y < \theta_f$ 和 $\theta_y < \theta_c$情況下,邊角流動和主要流動都出現在大 U 形槽中。此外,流動行為也受大 U 形槽長度(l_e)影響,對於尾端封閉之瞬間擴張管道,可以得到類似的分類結果,但是當l_e足夠小時,第三種情況的結果會改變,且最終可以填滿管道擴大的部分。
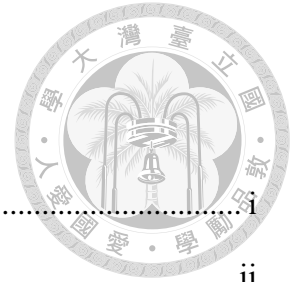
關鍵字:毛細現象; 開放式微流道; 矩形 U 形槽; Concus-Finn filament; 瞬間管道擴張

ABSTRACT
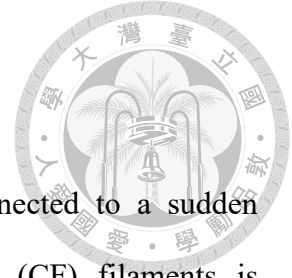
Imbibition dynamics in a rectangular U-groove that is connected to a sudden enlargement and complicated by the presence of Concus-Finn (CF) filaments is investigated using many-body dissipative particle dynamics. For open-ended sudden enlargement, four flow types are identified and depend on the contact angle θ_y, critical angle θ_f associated with CF filaments, and critical angle θ_c associated with the main flow. Firstly, for $\theta_y > \theta_f$ and $\theta_y > \theta_c$, the corner flow is absent, and the main flow stops at the end of the small U-groove. Secondly, for $\theta_c > \theta_y > \theta_f$, the corner flow vanishes, but the main flow occurs. Thirdly, for $\theta_f > \theta_y > \theta_c$, the corner flow takes place in the large U-groove, but the main flow is still absent. Fourthly, for $\theta_y < \theta_f$ and $\theta_y < \theta_c$, both the corner and main flows appear in the large U-groove. Additionally, the flow dynamics is greatly influenced by the length of the large U-groove (l_e). For closed-ended sudden enlargement, similar findings can be obtained. However, the outcome of the third case is altered for sufficiently small l_e, and the sudden enlargement can eventually be filled.

Keywords: Capillary flow; Open microchannel; Rectangular U-groove; Concus-Finn filament; Sudden enlargement.

CONTENTS

LIST OF FIGURES

LIST OF TABLES

Chapter 1 Introduction

Capillary imbibition or capillary-driven flow describes liquid propagation into small pores induced by the surface interactions between the imbibing liquid and the walls.[1-4] Because the assistance of an additional actuation mechanism is not required,[5] capillary imbibition receives great attention, and it has various industrial applications, including oil recovery in shale reservoirs[6-7] and oil-water separation based on solid foams.[8] Recently, capillary action has been widely applied in the biomedical and diagnostic domains.[9-11] In these domains, open microfluidic capillary systems are commonly seen owing to the advantages of improved fluid accessibility and easier fabrication by utilizing lithography or 3D printing.[10] In addition, the utilization of open channels brings about the benefits of facile surface modification and preventing bubble formation, both of which can affect the flow characteristics in closed systems significantly.[10]

The simplest open microfluidic capillary system involves only a single air-liquid interface, and it can have various channel geometries, including V-groove, U-groove, and trapezoidal channels.[2,10] Among all geometries, rectangular U-grooves are commonly used in microfluidic devices because of easy fabrication[10] and large surface area-to-volume ratio.[12] In fact, rectangular U-grooves can provide efficient heat transfer and can be used in micro-cooling systems for electronic devices.[12] Therefore, the studies of flow dynamics in such a geometry are frequently reported.[2,13-19] The capillary flow dynamics in a rectangular U-groove is generally described by the modified Lucas-Washburn model, which assumes a flat upper liquid-air interface[13,15-19]

$$L^2 = k_m t, \tag{1}$$

where $k_m = 2\gamma H\zeta(\lambda)[\cos\theta_y(1 + 2\lambda) - 1]/3\mu$ where γ and μ are surface tension and viscosity, respectively. $\lambda = H / W$ represents the aspect ratio of the channel depth to width, θ_y denotes the equilibrium contact angle, and $\zeta(\lambda)$ is a function of the channel

1

aspect ratio. However, due to the complicated free-surface morphology, the modified Lucas-Washburn model shows poor agreement with experiments at small λ.[16] Recently, the lubrication-theory-based model gives a better agreement with experiments at small λ, but its prediction becomes worse with increasing θ_y ($\rightarrow 45°$) since the axial curvature gradient of the interface is neglected.[16] The experiments were carried out in a lithography-based rectangular microchannel with a programmed microstepping motor and high-speed camera for various values of λ.[16]

In an open rectangular U-groove, there are channel corners with sharp edges, which lead to the development of Concus-Finn (CF) filaments,[2,20-26] which are formed in sharp corners.[2,20,24] Note that liquid filaments also form in the corner of a close rectangular channel.[27,28] The criterion for the formation of liquid filaments in the corner depends on both the contact angle and wedge angle (2α),

$$\theta_y < \theta_f = \pi/2 - \alpha, \tag{2}$$

where θ_f depicts the critical angle associated with CF filaments.[2,21] If a droplet is deposited on the sharp corner, an endless growing filament will be observed if eq. (2) is satisfied.[2] That is, the surface free energy associated with the concave liquid–gas interface decreases continuously with increasing the radius of curvature of the droplet, corresponding to continuous liquid spreading in the corner and no bounded solution of the Young-Laplace equation.[22,25] The propagation of the corner flow is shown to obey $t^{1/2}$ scaling in the absence of gravity.[26] In contrast, if $\theta_y > \theta_f$, a static filament will be observed, and the bounded solution exists.[22,25] For an open rectangular U-groove ($\alpha = 45°$), CF filaments will appear in the corners if the liquid has a contact angle less than $\theta_f = 45°$. In capillary-flow experiments with $\theta_y < \theta_f$, CF filaments are observed to be ahead of the main capillary flow,[10,14] and they may influence fluid propagation.[10,20] Recently, steady-state rivulets are shown to exist in wedges when surface forces

2

(disjoining pressure) are accounted for, even as eq. (2) is satisfied.[23]

The use of rectangular U-grooves has been extended to various new applications, such as cell trapping[29-32] and thermal management[12,33-35] by altering their structures from uniform channels[12,31,33,35] to non-uniform ones,[29,32,34] even to channels with the sudden contraction[29,34] or enlargement.[29,30,32,33,34] The general criteria and flow dynamics associated with capillary imbibition have been analyzed experimentally and theoretically.[2,16,36-43] For capillaries with sharp edges, however, CF filaments may appear, and thus the flow dynamic becomes complicated. To prevent the existence of CF filaments, the rounded shape is employed for capillary channels and for the junction between small and large grooves (sudden enlargement).[12,39,44] Consequently, capillary flows in open channels with sharp vertical edges with or without the sudden enlargement still lack detailed explorations. In this work, an open rectangular U-groove with sudden enlargement is considered, and the junction also consists of sharp edges. The imbibition dynamics in such channels is explored by many-body dissipative particle dynamics (MDPD) simulations. To ensure the validation of our MDPD approach, the simulation outcomes are compared with the experimental results[16] in open rectangular U-grooves without the sudden enlargement first. Then, the time evolutions of the meniscus position and total imbibed mass are monitored for rectangular U-grooves with sudden enlargement. The corner flow associated with CF filaments is especially accounted for. The influences of surface wettability (θ_y) and the length of the open-ended sudden enlargement are investigated. Four different flow types can be clearly identified. Finally, a closed-ended sudden enlargement is studied, and the result is compared with that of an open-ended sudden enlargement.

3

Chapter 2 Simulation Methods
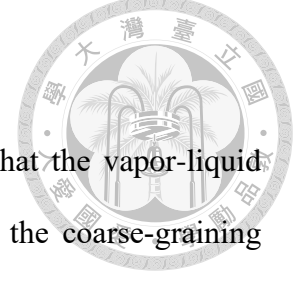
MDPD is modified from conventional DPD simulations so that the vapor-liquid coexistence can be achieved.[45-47] In MDPD or DPD simulations, the coarse-graining treatment is adopted, and mesoscopic effects can be studied.[45,48] Every particle in the MDPD system depicts a cluster of molecules and has mass m. The motion of the particle is governed by three forces, including conservative force (F_{ij}^C), dissipation force (F_{ij}^D), and random force (F_{ij}^R). F_{ij}^C in MDPD includes attraction and local-density-dependent repulsion,

$$F_{ij}^C = a_{ij}\omega_c(r_{ij})\hat{r}_{ij} + b_{ij}\left(\rho_i + \rho_j\right)\omega_d(r_{ij})\hat{r}_{ij}, \tag{3}$$

where the interaction parameters $a_{ij} < 0$ and $b_{ij} > 0$ denote the attractive and repulsive strengths between particles i and j, respectively. r_{ij} denotes the distance between the two beads and $\hat{r}_{ij}$ denotes the unit vector in the direction of the separation. The weight functions are $\omega_c(r_{ij}) = 1\text{-}r_{ij}/r_c$ and $\omega_d(r_{ij}) = 1\text{-}r_{ij}/r_d$, where r_c and r_d represent the range of attraction and repulsion, respectively. Both of them decrease linearly with the interparticle distance and vanish as r_{ij} exceeds the interaction range r_c or r_d.[45,49] ρ_i represents the local density associated with the particle i, and it is defined as

$$\rho_i = \frac{15}{2\pi r_d^3}\sum_{j\neq i}\left(1 - \frac{r_{ij}}{r_d}\right)^2, \text{ if } r_{ij} < r_d; \quad 0, \text{ if } r_{ij} > r_d. \tag{4}$$

F_{ij}^D and F_{ij}^R are the same as DPD,[1,46,48,50] $F_{ij}^D = \delta\omega^D(\hat{r}_{ij}\text{-}v_{ij})\hat{r}_{ij}$ and $F_{ij}^R = -\sigma\omega^R\xi_{ij}\hat{r}_{ij}$, where v_{ij} is the relative velocity of bead i with respect to bead j. δ denotes the friction coefficient, $\sigma = (2\delta k_B T)^{1/2}$ the noise amplitude, and ξ_{ij} a random number with zero mean. ω^D and ω^R are r_{ij}-dependent weight functions and $\omega^D = (\omega^R)^2 = (1 - r_{ij}/r_c)^2$ is chosen to satisfy the fluctuation-dissipation theorem.[50] To fullfill the no-slip boundary condition, F_{ij}^D between liquid and solid particles is set six times as F_{ij}^D between liquid particles.[1,45] The MDPD simulation is operated in reduced units, and all quantities are non-

4

dimensionalized by the thermal energy k_BT, particle mass m, and cutoff distance (particle size) r_c. For instance, the velocity can be scaled by $\sqrt{k_BT/m}$ and the time t by $\sqrt{mr_c^2/k_BT}$.

In this work, three types of open microchannels are considered, and all of them are connected to a reservoir subject to the periodic boundary condition in the x and y directions, as shown in Fig. 1 where only part of the reservoir is shown. To prevent liquid from climbing the outer walls of the rectangular channels, horizontal walls are placed atop the reservoir. The first type is an open rectangular U-groove composed of three walls, as illustrated in Fig. 1(a). The channel length is $l_t = 85$, the channel width W = 5 or 11, and the channel depth H = 2.5 or 4.5. The effects of three aspect ratios λ = H / W are studied. The second type is a small rectangular U-groove (l = 42.5, W = 5, and H = 2.5) connected with a large U-groove (open-ended sudden enlargement), as demonstrated in Fig. 1(b). The length and width of the large U-groove are denoted by l_e (10, 30, and 75) and w_e (0.5, 9, and 18), respectively. The third type is the same as the second one, but the sudden enlargement has a closed end, as depicted in Fig. 1(c). The large U-groove has a length of l_e = 15 or 30 and a width w_e = 18.

All the solid walls are made of three layers of fixed MDPD particles, and the number density is 8. The total number of liquid particles (N) is 84000, and the number density is 6. The cutoff distances of r_c and r_d are chosen as 1.0 and 0.75, respectively. The repulsive interaction parameter for all interaction pairs is set as b_{ij} = 25 to satisfy the no-go theorem.[51] The attractive interaction parameter is chosen as a_{ll} = -40 for attraction between liquid particles. However, it is varied from a_{sl} = -36 to -39.9 for attraction between solid and liquid particles to display different surface wettability in terms of contact angles θ_y = 18 ~ 55°,[45] The MDPD time step is set as Δt = 0.01 and 4×10^5 steps are run to ensure the equilibrium condition in the reservoir before wicking. After the reservoir reaches its equilibrium state, the open U-groove channel is placed atop the

5

reservoir to allow imbibition for at least 2×10^6 steps. During the imbibition process, the meniscus position L(t) and total imbibed mass Q(t) are monitored. The meniscus position L(t) is determined by the meniscus front near the center (y = 0) and the bottom of the microchannel, where the liquid particles just vanish.
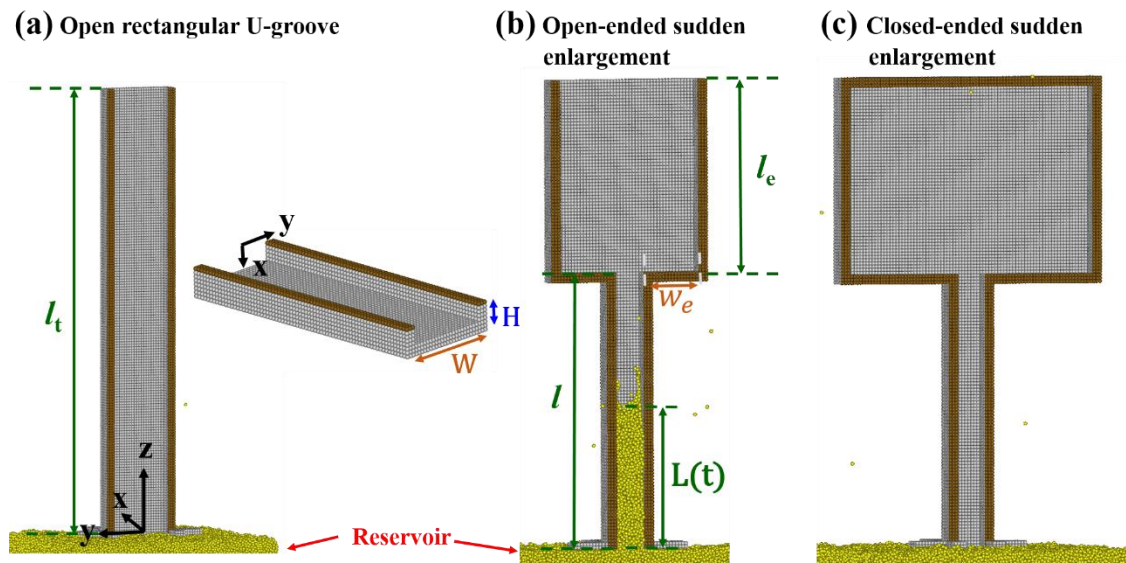

Figure 1. Schematics of (a) top and side views of an open rectangular U-groove, and top views of a small rectangular U-groove connected with (b) an open-ended sudden enlargement, and (c) a closed-ended sudden enlargement.

Chapter 3 Results and discussion

3.1 Validation of MDPD approach

Capillary flows of non-volatile liquids in open rectangular channels with the channel length l_t have been observed experimentally for different aspect ratios ($\lambda = H / W$).[16] To validate the MDPD approach, the experimental results are compared to our simulation outcomes for the evolution of the meniscus position L(t) and free-surface morphology. Figure 2 shows the comparisons between experiments and simulations for L(t) based on the dimensionless length and time, $(L/l_t)^2$ and $t/(\mu l_t^2/\gamma H)$. Here γ and μ denote the surface tension and viscosity, respectively. The range of the experimental result of L(t) is represented by the shaded area bounded by the dashed lines. Four experimental conditions are considered: silicone oil ($\theta_y = 18°$) at $\lambda = 0.23$ and 0.9 depicted in Fig. 2(a) and propylene glycol ($\theta_y = 42°$) at $\lambda = 0.3$ and 0.9 in Fig. 2(b). As reported in the previous study,[16] the lubrication-theory-based model fails to predict the case of propylene glycol with $\lambda = 0.3$, and the modified Lucas-Washburn model is unable to describe the two cases: silicone oil with $\lambda = 0.23$ and propylene glycol with $\lambda = 0.9$. In contrast, all aforementioned experimental results can be well captured by our MDPD simulations. It should be noted that increasing the simulation system's size does not affect the findings, suggesting that the simulation system's dimensions are sufficient to prevent any size effect.

In addition to the evolution of the meniscus position, the free-surface morphology is also examined for comparison. Dependent on the critical aspect ratio (λ_c), the experiments demonstrate two types of free-surface morphology which can be divided into three regimes. Consistent with the experimental observations, Fig. 3(a) and (b) illustrate the two types of free-surface morphology (the colorbar represents the variation in channel depth) acquired from MDPD simulations for $\theta_y = 18°$ with $\lambda = 0.23$ and 0.63. Here $\lambda_c = (1 - \sin\theta_y)/2\cos\theta_y = 0.36$. As $\lambda > \lambda_c$, the regimes include (I) meniscus-deformation

7

(pinned to the top of channel walls), (II) meniscus-recession (depinning from the top of sidewalls), and (III) corner flow. As $\lambda < \lambda_c$, the regime (II) is replaced by the regime (IV) corner-transition (pinned to the top of sidewalls after splitting the meniscus). Evidently, the good agreement between experiments and simulations for open rectangular microchannels verifies the validation of our MDPD approach.

(a) Silicone oil
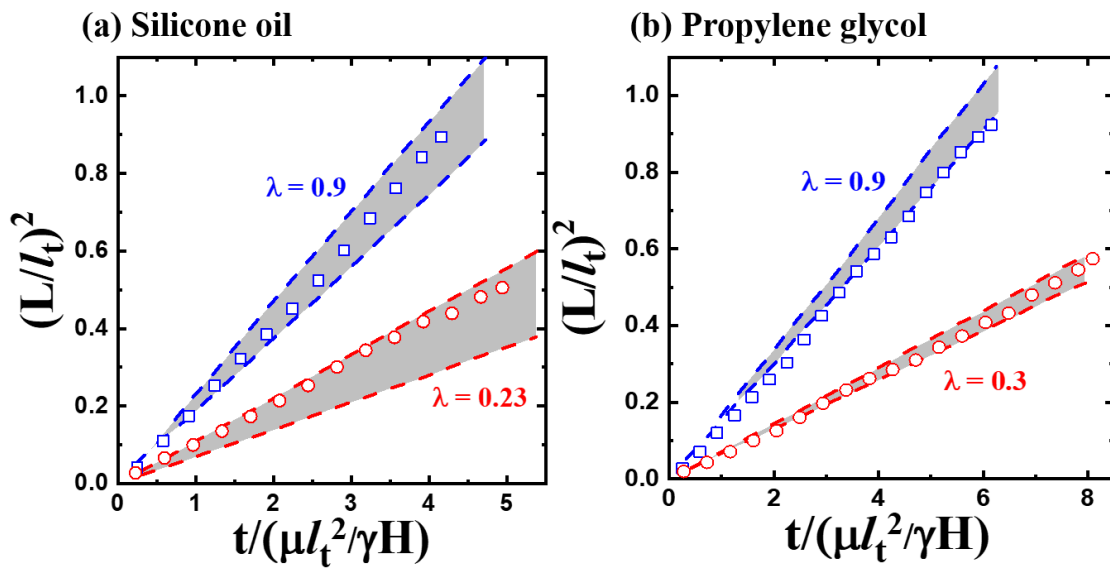
(b) Propylene glycol

Figure 2. Comparisons between experiments[16] and simulations for the meniscus position $L(t)$ based on the dimensionless length and time, $(L/l_t)^2$ and $t/(\mu l_t^2/\gamma H)$. (a) silicone oil ($\theta_y = 18°$, $\lambda = 0.23$ and 0.9); (b) propylene glycol ($\theta_y = 42°$, $\lambda = 0.3$ and 0.9). Simulation data are represented by symbols and experimental results are within two dash lines.

(a)
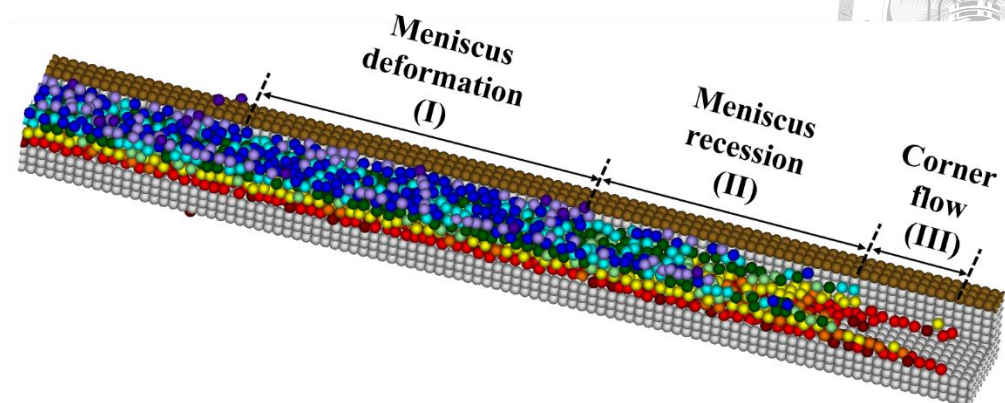
(b)
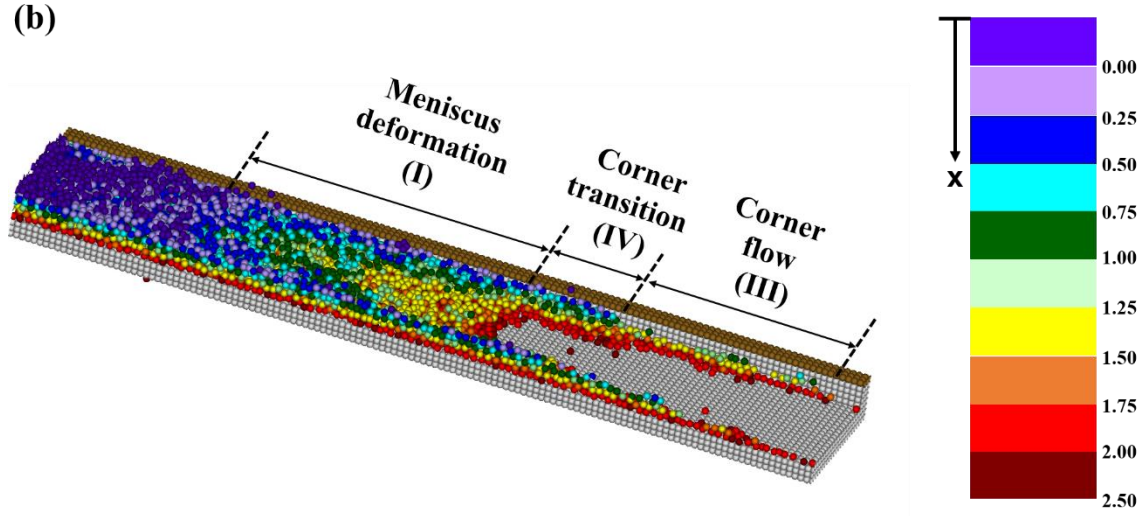
Figure 3. Free-surface morphology acquired from MDPD simulations with $\theta_y = 18°$ ($\lambda_c = 0.36$) for two conditions, (a) $\lambda = 0.63$ ($\lambda > \lambda_c$) and (b) $\lambda = 0.23$ ($\lambda < \lambda_c$).

9

3.2 Capillary flow into a sudden enlargement with an open end

3.2.1 The critical contact angle for imbibition

Consider a straight U-groove exiting to a rectangular enlargement with the width w_e as depicted in Fig. 1(b). The U-groove and enlargement have the same depth H = 2.5 and their connection contains sharp vertical edges. Whether the capillary flow is stopped at the en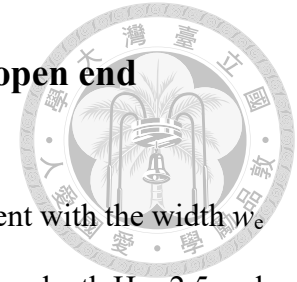trance of the enlargement or not can be determined by the surface free energy analysis.[2,37] By considering the rectangular enlargement as a U-groove, the condition for spontaneous capillary flow into the enlargement is similar to the condition for wicking in a U-groove with CF filaments ($\theta_y < \theta_f = 45°$),[2]

$$\frac{2w_e + W}{H} \le \frac{2\sin\theta_y}{1 - \cos\theta_y},$$ (5)

where θ_y must be less than the critical contact angle θ_c for spontaneous imbibition. If CF filaments are absent ($\theta_y > 45°$), the condition for wicking becomes[2]

$$\frac{2w_e + W}{H} \le \frac{2\cos\theta_y}{1 - \cos\theta_y}.$$ (6)

According to eqs. (5) and (6), the critical contact angle is $\theta_c = 24.5°$ and 34.8° for $w_e = 9$, W = 5, and H = 2.5, respectively. Figure 4(a) shows the imbibition dynamics in terms of the meniscus position L(t) for liquids with two different contact angles, $\theta_y = 32°$ (with CF filaments) and 55° (without CF filaments). Consistent with the modified Lucas-Washburn equation, the dynamics before reaching the enlargement can be well described by $L(t)^2 = k_m t$. The slope k_m decreases with increasing θ_y. Evidently, the capillary flow is stopped at the channel end for $\theta_y = 55° > \theta_c = 34.8°$ (weaker wettability) and it cannot enter the cavity, which is illustrated by a constant L(t). This outcome agrees with eq. (6) and the sudden enlargement can act as a capillary valve.[2,39,52] $\theta_y = 55°$ can be smaller than the critical contact angle $\theta_c = 57°$ based on eq. (6) as the width of the sudden enlargement is significantly reduced to $w_e = 0.5$. Under this condition $\theta_c > \theta_y > \theta_f$, the

10

capillary flow will continue from the small U-groove into the sudden enlargement.
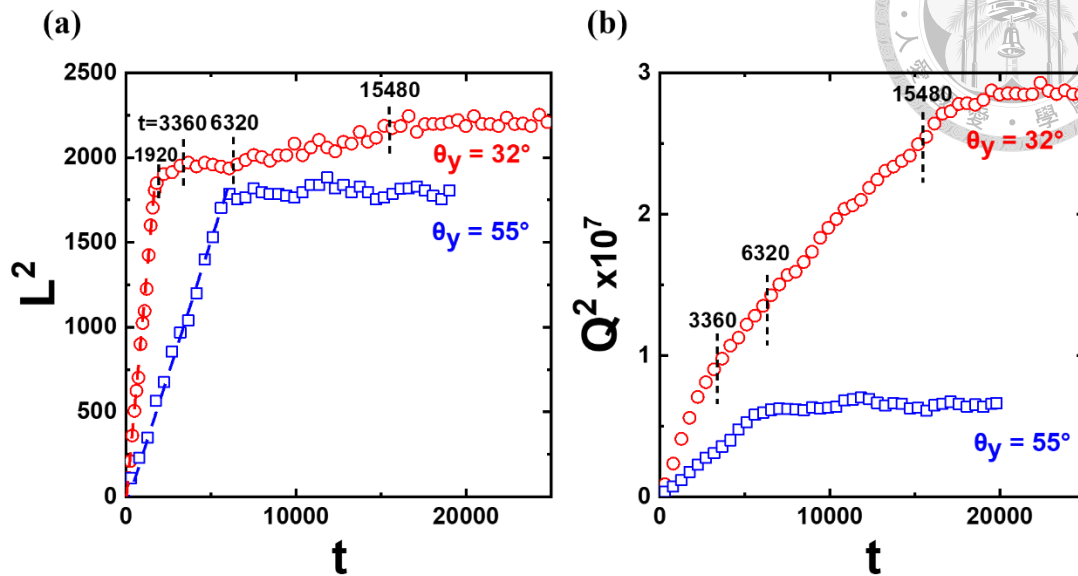

Figure 4. The time evolution of (a) the square of the meniscus position $L^2(t)$ and (b) the square of the total imbibed mass $Q^2(t)$ for liquids for with $\theta_y = 32°$ and $55°$ at $w_e = 9$ and $l_e = 30$.

According to eq. (5) the capillary flow into the sudden enlargement is not allowed for $\theta_y = 32°$ ($\theta_c = 24.5°$) as well. As shown in Fig. 4(a), when the meniscus reaches the small channel end, its position increases slightly (t = 1920 ∼ 3360) and is then halted. Although the condition of constant L lasts for a while (t = 3360 ∼ 6320), the second slight increase of L(t) is observed (t = 6320 ∼ 15480) and becomes unchanged eventually. Figure 5 shows that an adjustment of the meniscus in the large U-groove is associated with the sudden enlargement, and it is driven by the corner flow (CF filaments). This phenomenon occurring for $\theta_y = 32°$ is not observed for $\theta_y = 55°$. The first slight increase in Fig. 4(a) for $\theta_y = 32°$ is due to the corner flow along the y-direction in the large U-groove. The arrest period is associated with a stop of the main capillary flow but with the corner flow developing along the z-direction. After the z-direction corner flow

11

reaches the end of the large U-groove, the meniscus starts to adjust itself, leading to the second increase of L(t).
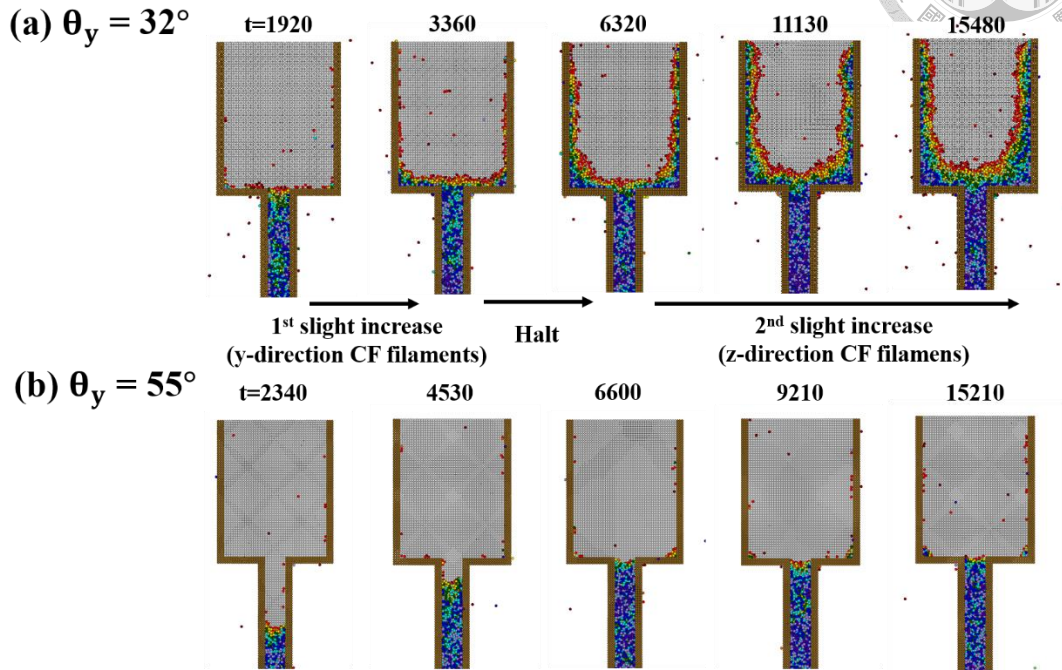
Figure 5. Adjustment of the meniscus as the capillary flow reaches the sudden enlargement with $w_e = 9$ and $l_e = 30$ for (a) $\theta_y = 32^o$ and (b) $\theta_y = 55^o$.

To show the continuous corner flow (CF filaments), the total imbibed mass Q(t) associated with the capillary flow is introduced. As shown in Fig. 4(b), Q(t) for $\theta_y = 55°$ ceases to change and becomes a constant as the flow arrives at the end of the small U-groove. Evidently, the result of Q(t) is consistent with that of L(t). However, it is found that Q(t) for $\theta_y = 32°$ still grows with time continuously even when L(t) is arrested. This consequence indicates that the corner flow is significant for $\theta_y = 32°$ but not for $\theta_y = 55°$. The above results are consistent with criterion eq. (2) for the wedge angle of $2\alpha = 90°$. That is, CF filaments emerge only as $\theta_y < \theta_f = 45°$.

12
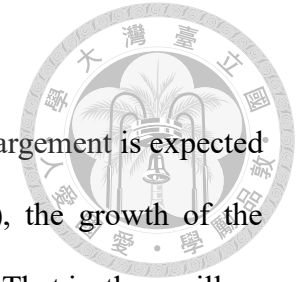
3.2.2 Endless-growing CF filaments

In contrast to $\theta_y = 32°$ and 55°, the capillary flow into the enlargement is expected for $\theta_y = 18° < \theta_c$ (stronger wettability). As shown in Fig. 6(a), the growth of the meniscus position can be observed after an arrest of L(t) for a while. That is, the capillary flow seems to be temporarily halted (e.g., t = 2520 ~ 5280 for $l_e = 30$) after the first slight increase of the meniscus position (t = 1440 ~ 2520). Evidently, five regimes can be clearly identified in the plot of L(t): flow in the small U-groove, first slight increase, arrest period, second slight increase, and flow in the large U-groove. In contrast with L(t), the arrest period is not shown in the plot of Q(t) depicted in the inset of Fig. 6(a). Similar to the scenario of $\theta_y = 32°$, this continuous growth of the total imbibed mass reveals that the corner flow (CF filaments) persists even as the main capillary flow is halted by the sudden enlargement. As demonstrated in Fig. 6(b), the z-direction corner flow in the large U-groove takes place during the arrest period, and the second slight increase is associated with the meniscus adjustment. After the meniscus is fully developed in the large U-groove, the meniscus position advances again, revealing that the main capillary flow resumes.

It seems that in the large U-groove, the occurrence of the main capillary flow is dependent on the developing process of the meniscus, which is affected by the corner flow (CF filaments). Since the range of the meniscus reaches the end of the large U-groove (see Fig. 6(b)), the length of the large U-groove (l_e) has to come into play. To examine the influence of l_e, the imbibition dynamics of different channel lengths ($l_e = $ 10, 25, and 75) are performed for $\theta_y = 18°$ at the same length of the small U-groove ($l = $ 42.5). As shown in the inset of Fig. 7(a), for the short channel length $l_e = $ 10, the arrest period is very short (t = 2520 ~ 3720), and the meniscus of the main flow arrives at the channel end quickly (t ~ 10000). Consequently, the regimes of the second slight increase and the main capillary flow cannot be clearly distinguished. On the contrary, for the long

13
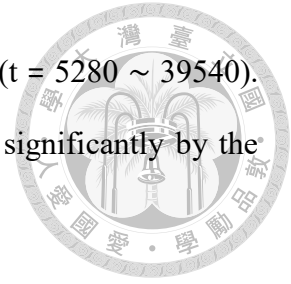
channel length $l_e = 75$, the second slight increase lasts very long (t = 5280 ~ 39540). Evidently, the duration of the second slight increase is influenced significantly by the length of the large U-groove.

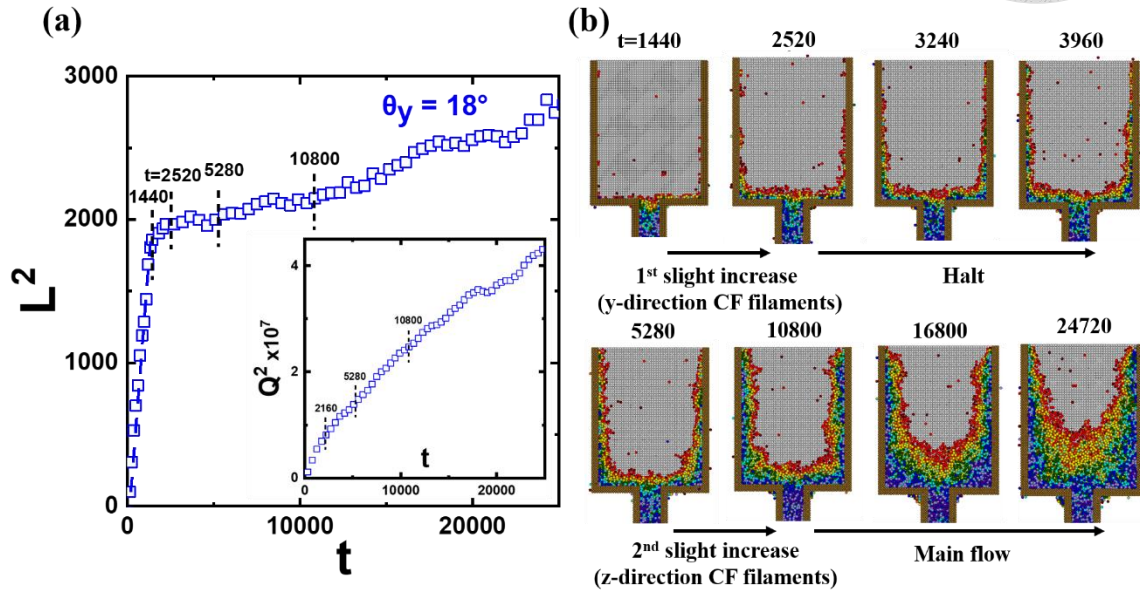Figure 6. (a) The time evolution of the square of the meniscus position $L^2(t)$ and the square of the total imbibed mass $Q^2(t)$ for liquid with $\theta_y = 18^o$. (b) Adjustment of the meniscus as the capillary flow reaches the sudden enlargement with $w_e = 9$ and $l_e = 30$.

According to Fig. 6(b), the onset of the main capillary flow from the sudden enlargement can be related to the development of the corner flow (CF filaments) at the large U-groove. Since it takes a longer time for the corner flow with a longer length l_e to reach the end of the channel and to become fully developed, the beginning of the main capillary flow has to wait longer. This result is somewhat surprising because the main flow is not expected to occur in an infinitely long large U-groove, even as $\theta_y < \theta_c$. To understand the role of the corner flow further, the variation of the total imbibed mass with time Q(t) is monitored as well for different channel lengths, as illustrated in Fig. 7(b). The contribution to Q comes from the main capillary flow and corner flow. The cessation of

14

both the main and corner flows is clearly observed by time-invariant Q for the short channel length $l_e = 10$. In contrast, Q continues to grow with time for both $l_e = 25$ and 75. In the former, the main flow resumes after the second slight increase (t > 10080). In the latter, the corner flow continues while the meniscus of the main flow is arrested. It is interesting to find that the growth rate of Q for $l_e = 75$ is higher than that for $l_e = 25$, indicating that the mass flowrate of the corner flow is greater than that of the main capillary flow. This consequence implies that in an infinitely long U-groove associated with the sudden enlargement, the corner flow prevails over the main flow because the former is more effective than the latter in terms of mass transport.
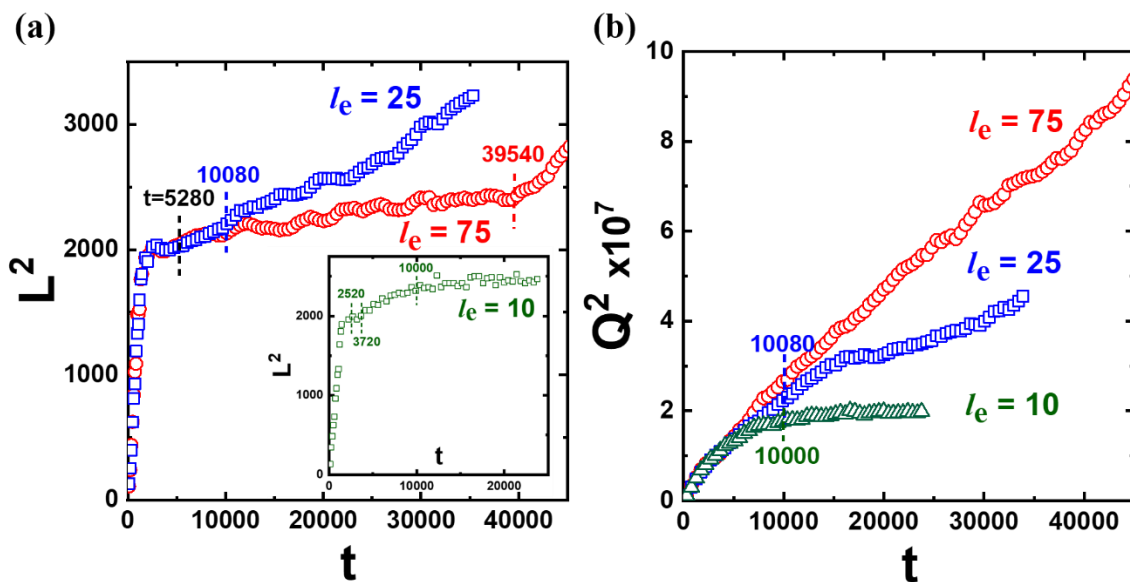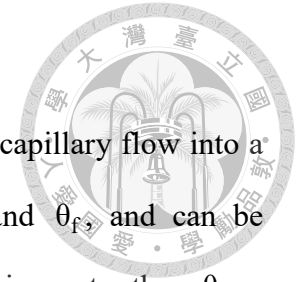

Figure 7. The time evolution of (a) the square of the meniscus position $L^2(t)$ and (b) the square of the total imbibed mass $Q^2(t)$ for liquids with $\theta_y = 18^o$ at $w_e = 9$ and $l_e = 10$, 25 and 75.
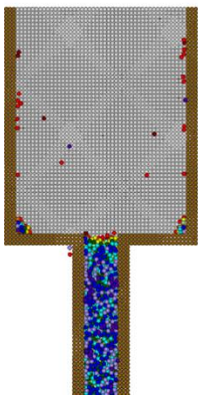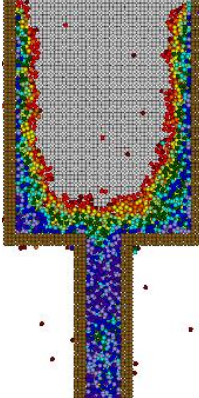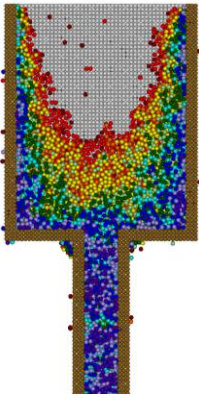
15

3.2.3 Four regimes based on θ_c and θ_f

According to the aforementioned results, the outcomes of the capillary flow into a sudden enlargement depend on the critical contact angles θ_c and θ_f, and can be classified into four scenarios. Firstly, in the case of $\theta_y = 55°$ which is greater than $\theta_c = 34.8°$ and $\theta_f = 45°$ at $w_e = 9$, the main flow is stopped by the sudden enlargement, and the corner flow is absent. Secondly, in the case of $\theta_y = 55°$ which is less than $\theta_c = 57°$ but larger than $\theta_f = 45°$ at $w_e = 0.5$, the main flow into the sudden enlargement can be observed, but the corner flow is still absent. Thirdly, in the case of $\theta_y = 32°$ which is larger than $\theta_c = 24.5°$ but lower than $\theta_f = 45°$ at $w_e = 9$, the main flow is halted by the sudden enlargement, but the corner flow persists in the large U-groove. Fourthly, in the case of $\theta_y = 18°$ which is less than both $\theta_c = 24.5°$ and $\theta_f = 45°$ at $w_e = 9$, both the main and corner flows appear in the large U-groove. Evidently, four conditions can be identified: (i) $\theta_y > \theta_c$ and $\theta_y > \theta_f$, (ii) $\theta_c > \theta_y > \theta_f$, (iii) $\theta_f > \theta_y > \theta_c$ and (iv) $\theta_y < \theta_c$ and $\theta_y < \theta_f$, and their flow types are summarized in Table 1.

Table 1. Four types of capillary flow into sudden enlargement based on θ_c and θ_f

	$\theta_y > \theta_c$ & $\theta_y > \theta_f$	$\theta_c > \theta_y > \theta_f$	$\theta_f > \theta_y > \theta_c$	$\theta_y < \theta_c$ & $\theta_y < \theta_f$
Corner flow	✘	✘	✓	✓
Main flow	✘	✓	✘	✓
Flow types				

16

3.3 Capillary flow into a sudden enlargement with a closed-end

The aforementioned results of $\theta_y = 32°$ indicates that for $\theta_y > \theta_c$ (eq. (5)), the main capillary flow into a sudden enlargement is halted; but owing to $\theta_y < \theta_f$ (eq. (2)), the corner flow (CF filaments) continues along the large U-groove. As a result, all the corners of the large U-groove will be occupied eventually. This consequence reveals that the sudden enlargement with a closed end may have a different outcome from that with an open end. Figure 8 demonstrates the imbibition process of the sudden enlargement with the open and closed ends for the same width $w_e = 18$ and length $l_e = 15$. According to eq. (5) the critical contact angle is $\theta_c = 13.9°$ for $w_e = 18$, and thus the capillary flow into the sudden enlargement is not allowed for $\theta_y = 32°$, as illustrated in Fig. 8(a) for an open end. However, for the sudden enlargement with a closed-end, the cavity can be completely filled ultimately, as depicted in Fig. 8(b), implying that capillary wicking can take place for $\theta_y > \theta_c$. Nonetheless, the filling process is quite different from the typical capillary flow. After all the corners surrounding the large U-groove are occupied by the corner flow (t = 7680), the solid-gas area in the center of the cavity shrinks gradually (t = 7680 ~ 67230). The exposed region vanishes eventually (t = 67230), and the cavity of the large U-groove is completely filled by the liquid.
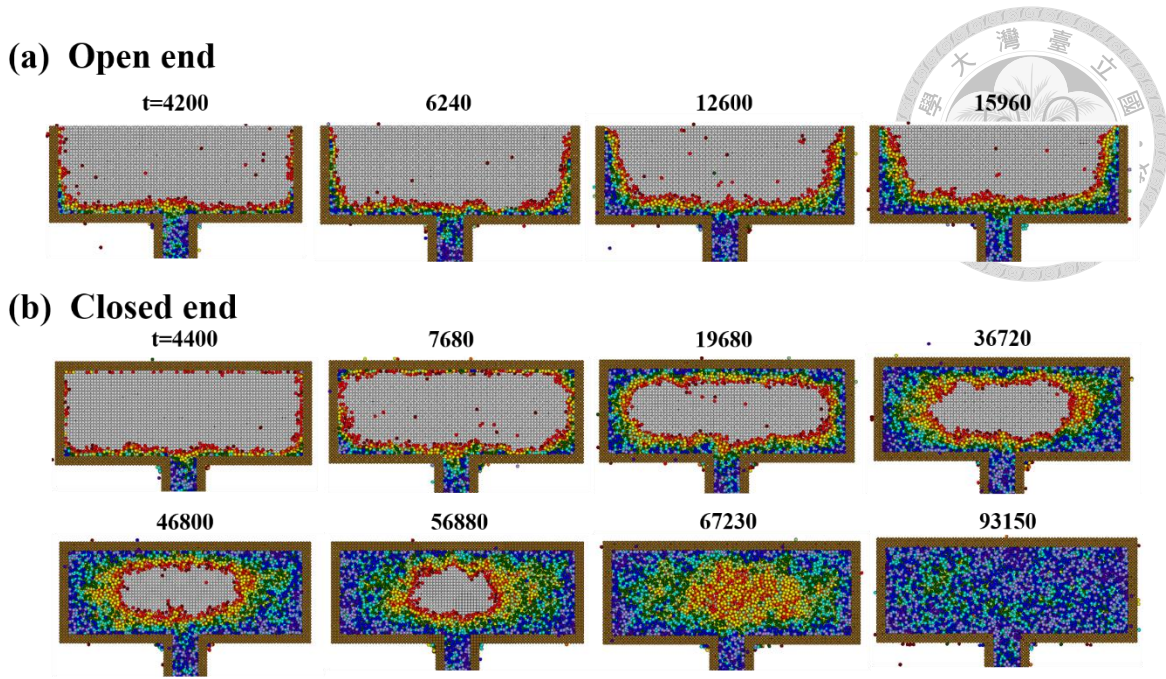
(a) Open end

(b) Closed end

Figure 8. The filling behavior as the capillary flow reaches the sudden enlargement with $w_e = 18$ and $l_e = 15$ for (a) open end and (b) closed end.

Evidently, the imbibition criterion ($\theta_y > \theta_c$) needs to be modified as the closed end of the sudden enlargement is considered. When $\theta_y > \theta_f$, the corner flow cannot occur, and the final outcome of the case $\theta_y > \theta_c$ is always no imbibition regardless of the open or closed end. However, as $\theta_f > \theta_y > \theta_c$, the occurrence of the corner flow (CF filaments) complicates the final result. After all the corners of the large U-groove are fully occupied by the corner flow, the meniscus tends to adjust itself so that the surface free energy of the system can be minimized. To demonstrate the development of the meniscus in the large U-groove, the time evolutions of L(t) at y = 0 (main capillary flow) and Q(t) are monitored for the case shown in Fig. 8. Figure 9 depicts the plots of L^2 and Q^2 against the time for the condition satisfying $\theta_f > \theta_y > \theta_c$. While the total imbibed mass grows with time continuously, the meniscus position (lower meniscus in the large U-groove) at y = 0 displays a sudden jump to reach the closed end of the large U-groove, which is associated with the very rapid decrease of the solid-gas area, as illustrated in Fig. 8 from

18

t = 56880 to 67230. This consequence indicates that complete imbibition of the large U-groove is not done by the typical capillary flow but accomplished by the corner flow and gradually wetting the bottom of the sudden enlargement.
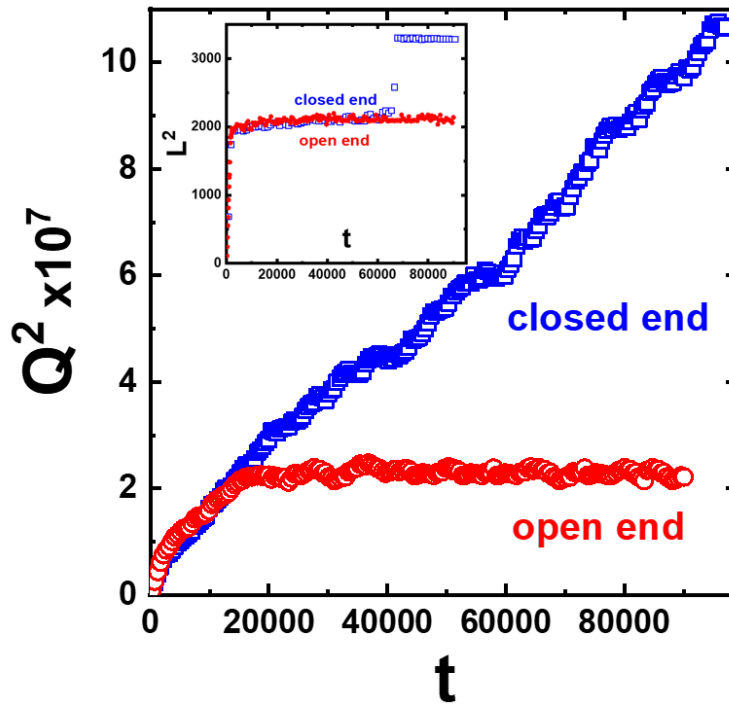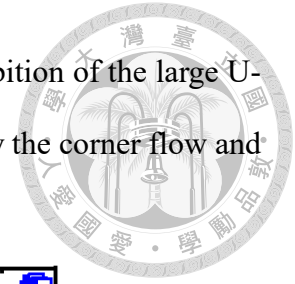

Figure 9. The time evolution of the square of the meniscus position $L^2(t)$ and the square of the total imbibed mass $Q^2(t)$ for liquid with $\theta_y = 32^\circ$ at $w_e = 18$ and $l_e = 15$.

The different outcomes between the sudden enlargement with an open end and that with a closed-end can be realized from the surface free energy analysis. As $\theta_f > \theta_y$, CF filaments always fill the corners regardless of the condition of the open or closed end. According to our simulations, the meniscus extends from the top of the sidewall toward the center of the large channel. For simplicity, the surface morphology of the meniscus is assumed as a planar plane characterized by an apparent contact angle θ,[2,53] as depicted in the supporting information of Fig. S1. The free energy of the fully filled state F_f^* and the partly filled state $F_p^*(\theta)$ for a closed end can be formulated in their dimensionless forms,

$$F_f^*(\theta) = \gamma_{LG}^* \{-\cos\theta_y [(2H + 2w_e + W)l_e + 2H(2w_e + W)] + (2w_e + W)l_e\}, \quad (7)$$

and

$$F_p^*(\theta) = \gamma_{LG}^* \{-\cos\theta_y [(2H + 2\frac{H}{\tan\theta})l_e + 2H(2w_e + W) + 2\frac{H}{\tan\theta_y}(2w_e + W - 2\frac{H}{\tan\theta})]$$

$$+[(2\frac{H}{\sin\theta})l_e + 2\frac{H}{\sin\theta_y}(2w_e + W - 2\frac{H}{\tan\theta})]\}. \quad (8)$$

Equations (7) and (8) are formulated based on the total surface free energy, $F = (\gamma_{SL} - \gamma_{SG})A_{SL} + \gamma_{LG}A_{LG}$, whose dimensionless form is $F^* = \gamma_{LG}^*[-\cos\theta_y A_{SL}^* + A_{LG}^*]$. The procedure for non-dimensionalization is identical to that of MDPD. Equaiton (7) represents the fully filled state, while equation (8) describes the partly filled state. The approximate surface areas (A_{SL}^* and A_{LG}^*) can be estimated for those two states.[53] The first term in eqs. (7) and (8) denotes the energy gain for wetting the solid wall, while the second term is the energy gain due to the new exposure to the gas phase. $\Delta F^* = F_f^* - F_p^*(\theta = \theta_y)$ can be used to determine whether the state of the completely filled cavity for $\theta_y > \theta_c$ is favored or not. To obtain $\Delta F^* < 0$, the length of the large U-groove l_e must be less than a critical value (l_e^*) so that the fully filled state is favored. As demonstrated in the supporting information of Fig. S2, for $\theta_y = 32°$, $l_e^* = 24$ can be determined from the condition of $\Delta F^* = 0$. Consequently, $l_e < l_e^* = 24$ must be satisfied to acquire a completely filled cavity. In fact, the partly filled state with CF filaments (no imbibition) is observed for $l_e = 30$. As $l_e < l_e^*$, the gradually extending meniscus corresponding to imbibition into a closed-ended sudden enlargement is accompanied by the continuously decaying surface free energy, $F_p^*(\theta)$, relative to $F_p^*(\theta = \theta_y)$ with decreasing θ, as illustrated in the supporting information of Fig. S3, indicating the totally filled state is the preferred condition. On the contrary, the surface free energy grows with decreasing θ in an open-ended enlargement, revealing that the uncovered state (see Fig. 8(a)) is favored.

Chapter 4 Conclusion

The imbition dynamics of liquid in open rectangular microchannels with sudden enlargement is explored by MDPD simulations. Without the sudden enlargement, the simulation results are in good agreement with experimental results for different contact angles and channel aspect ratios. This consequence verifies the validity of the MDPD approach for studying capillary flow in U-grooves. In the presence of sudden enlargement, the behavior of the imbition dynamics is investigated by monitoring the meniscus position L(t) and total imbibed mass Q(t), in addition to snapshots of free-surface morphology. It is found that the imbition behavior is controlled by the critical contact angles θ_c and θ_f associated with the stop of the main capillary flow and the occurrence of CF filaments, respectively. Besides, the final outcome of the spontaneous capillary flow depends also on the open or closed end of the sudden enlargement.

In an open-ended sudden enlargement, four cases can be identified. Firstly, for $\theta_y > \theta_f$ and $\theta_y > \theta_c$, the corner flow is absent, and the main flow is halted at the end of the small U-groove channel. Secondly, for $\theta_c > \theta_y > \theta_f$, the corner flow vanishes, but the main flow comes about. Thirdly, for $\theta_f > \theta_y > \theta_c$, the corner flow takes place in the large U-groove, but the main flow is still not present. Fourthly, for $\theta_y < \theta_f$ and $\theta_y < \theta_c$, both the corner flow and main flow appear in the large U-groove. Nonetheless, the main flow starts only as the corner flow reaches the end of the large U-groove, and therefore the flow behavior depends significantly on the length of the large U-groove (l_e). In a closed-ended sudden enlargement, the flow behavior is similar to that of the open-ended condition for sufficiently large l_e. However, if l_e is less than the critical length l_e^*, the outcome of the third case will be altered. Although the main flow comes to a halt, the cavity associated with the sudden enlargement can be completely filled by the corner flow to reduce surface free energy.
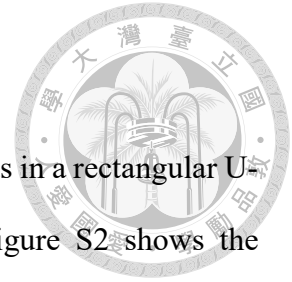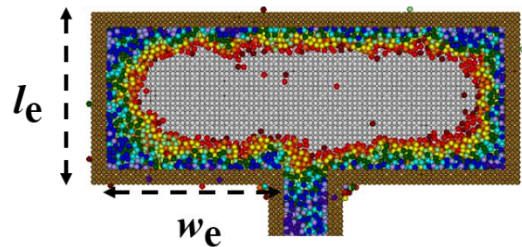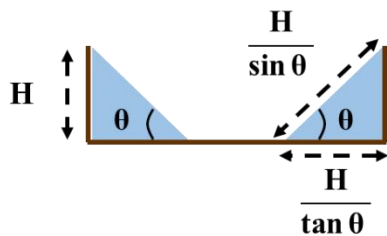
21

Chapter 5 Supporting information

Figure S1 shows schematics of the simple model of the meniscus in a rectangular U-groove with a closed end for surface free energy calculation. Figure S2 shows the variation of the surface free energy ΔF with the length of the enlargement l_e. Figure S3 demonstrates the variation of the surface free energy F_p with the apparent contact angle θ.

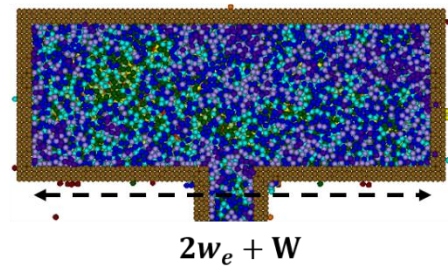## (a) Partially filled state

(b) Fully filled state
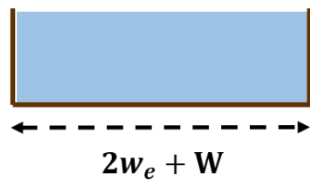
Figure S1. Schematics of the simple model of the meniscus in a rectangular U-groove with a closed end for surface free energy calculation. (a) Gradually changing meniscus characterized by θ and (b) fully filled cavity.

Figure S2. The variation of the surface free energy ΔF^* with the length of the enlargement l_e.
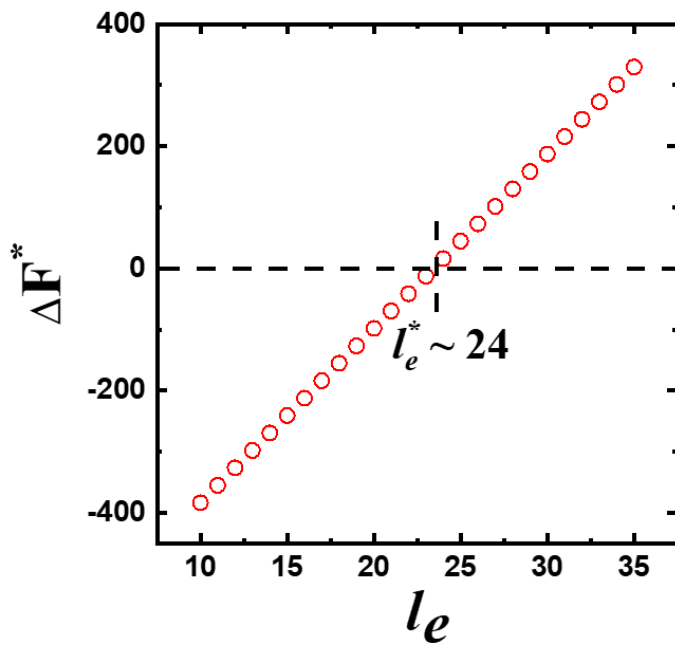
Parameters of eqs. (7) and (8):

$\gamma^*_{LG} = 7.5$

$\theta = \theta_y = 32°$

$H = 2.5$

$W = 5$

$l_e = 10 \sim 35$

$w_e = 18$

Figure S3. The variation of the surface free energy F^*_p with the apparent contact angle θ defined in Figure S1.

Parameters:

$\gamma^*_{LG} = 7.5$
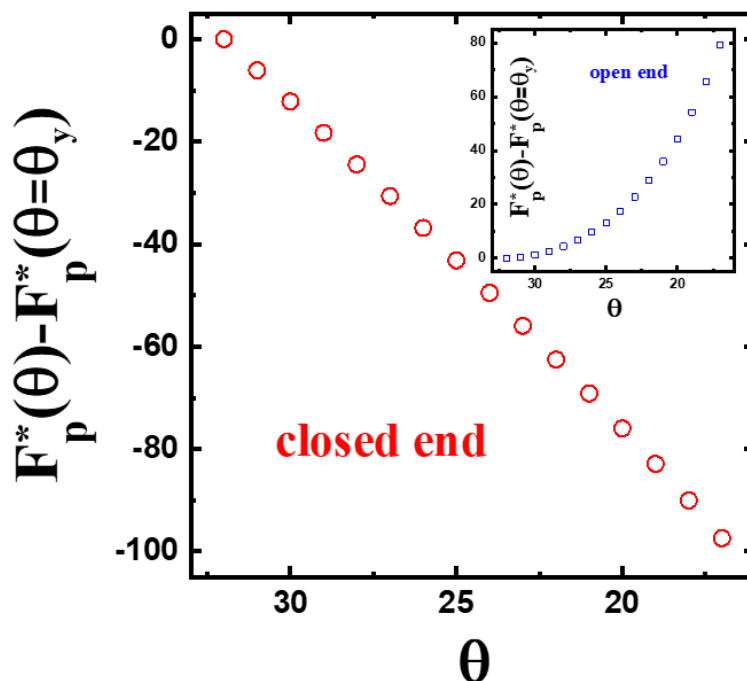
$\theta_y = 32°$

$\theta = 17° \sim 32°$
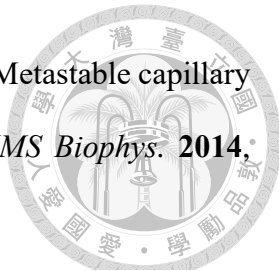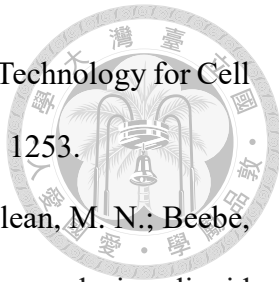
$H = 2.5$

$W = 5$

$l_e = 15$

$w_e = 18$

Reference

1. Berthier, J. *Micro-Drops and Digital Microfluidics* (Elsiver, 2013).

2. Berthier, J.; Brakke, K. A.; Berthier, E. *Open Microfluidics* (John Wiley & Sons, 2016).

3. Cheng, Y.-T.; Chang, H.-Y.; Tsao, H.-K.; Sheng, Y.-J. Imbibition dynamics and steady flows in graphene nanochannels with sparse geometric and chemical defects. *Phys. Fluids* **2022**, *34*, 112003.

4. He, G.-Y.; Tsao, H.-K.; Sheng, Y.-J. (2022) Imbibition dynamics in an open-channel capillary with holes. *J. Mol. Liq.* **2022**, *349*, 118117.

5. Berthier, J.; Brakke, K. A.; Furlani, E. P.; Karampelas, I. H.; Poher, V.; Gosselin, D.; Cubizolles, M.; Pouteau, P. Whole blood spontaneous capillary flow in narrow V-groove microchannels. *Sens. Actuators B Chem.* **2015**, 206, 258-267.

6. Andersson, J.; Larsson, A.; Ström, A. Stick–slip motion and controlled filling speed by the geometric design of soft micro-channels. *J. Colloid Interface Sci.* **2018**, 524, 139-147.

7. Li, C.; Singh, H.; Cai, J. Spontaneous imbibition in shale: A review of recent advances. *Capillarity* **2019**, 2(2), 17-32.

8. Behrens, S. H. Oil-coated bubbles in particle suspensions, capillary foams, and related opportunities in colloidal multiphase systems. *Curr. Opin. Colloid Interface Sci.* **2020**, 50, 10138.

9. Berlanda, S. F.; Breitfeld, M.; Dietsche, C. L.; Dittrich, P. S. Recent Advances in Microfluidic Technology for Bioanalysis and Diagnostics. *Anal. Chem.* **2021**, 93, 311-331.

10. Berthier, E.; Dostie, A. M.; Lee, U. N.; Berthier, J.; Theberge, A. B. Open microfluidic capillary systems. *Anal. Chem.* **2019**, 91(14), 8739-8750.
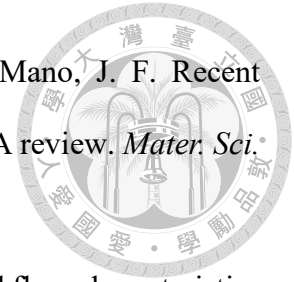
11. Oliveira, N. M.; Vilabril, S.; Oliveira, M. B.; Reis, R. L.; Mano, J. F. Recent advances on open fluidic systems for biomedical applications: A review. *Mater. Sci. Eng. C* **2019**, 97, 851-863.

12. Prajapati, Y. K. Influence of fin height on heat transfer and fluid flow characteristics of rectangular microchannel heat sink. *Int. J. Heat Mass Transf.* **2019**, 137, 1041–1052.

13. Baret, J. C.; Decre, M. M. J.; Herminghaus, S.; Seemann, R. Transport dynamics in open microfluidic grooves. *Langmuir* **2007**, 23(9), 5200-5204.

14. Gurumurthy, V. T.; Roisman, I. V.; Tropea, C.; Garoff, S. Spontaneous rise in open rectangular channels under gravity. *J. Colloid Interface Sci.* **2018**, 527, 151-158.

15. Kolliopoulos, P.; Jochem, K. S.; Lade Jr., R. K.; Francis, L. F.; Kumar, S. Capillary Flow with Evaporation in Open Rectangular Microchannels. *Langmuir* **2019**, 35, 8131−8143.

16. Kolliopoulos, P.; Jochem, K. S.; Johnson, D.; Suszynski, W. J.; Francis, L. F.; Kumar, S. Capillary-flow dynamics in open rectangular microchannels. *J. Fluid Mech.* **2021**, 911, A32.

17. Ouali, F. F.; McHale, G.; Javed, H.; Trabi, C.; Shirtcliffe, N. J.; Newton, M. I. Wetting considerations in capillary rise and imbibition in closed square tubes and open rectangular cross-section channels. *Microfluid.* **2013**, 15(3), 309-326.

18. Sowers, T. W.; Sarkar, R.; Prameela, S.; Izadi, E.; Rajagopalan, J. Capillary driven flow of polydimethylsiloxane in open rectangular microchannels. *Soft Matter* **2016**, 12(26), 5818–5823.

19. Yang, D.; Krasowska, M.; Priest, C.; Popescu, M. N.; Ralston, J. Dynamics of capillary-driven flow in open microchannels. *J. Phys. Chem. C* **2011**, 115 (38), 18761-18769.

20. Berthier, J.; Brakke, K. A.; Gosselin, D.; Huet, M.; Berthier, E. Metastable capillary filaments in rectangular cross-section open microchannels. *AIMS Biophys.* **2014**, 1(1), 31–48.

21. Concus, P.; Finn, R. On the behavior of a capillary surface in a wedge. *Proc. Natl. Acad. Sci. U.S.A.* **1969**, 63, 292-299.

22. Han, Z.; Duan, L.; Kang, Q. Behavior of a liquid drop in a rounded corner: Different contact angles. *AIP Advances* **2019**, 9, 085203.

23. Kubochkin, N.; Gambaryan-Roismana, T. Edge wetting: Steady state of rivulets in wedges. *Phys. Fluids* **2022**, 34, 042112.

24. Myra, K. B.; Marmur, A.; Trabold, T.; Dadheech, G. V. Groovy Drops: Effect of Groove Curvature on Spontaneous Capillary Flow. *Langmuir* **2007**, 23, 8406-8410.

25. Nikolai, K.; Tatiana, G. R. Capillary-driven flow in corner geometries. *Curr. Opin. Colloid Interface Sci.* **2022**, 59, 101575.

26. Zhou, J.; Doi, M. Universality of capillary rising in corners. *J. Fluid Mech.* **2020**, 900, A29.

27. Zhao, J.; Qin, F.; Fischer, R.; Kang, Q.; Derome, D.; Carmeliet, J. Spontaneous imbibition in a square tube with corner films: Theoretical model and numerical simulation. *Water Resour. Res.* **2021**, 57, e2020WR029190.

28. Zhao, J.; Qin, F.; Kang, Q.; Qin, C.; Derome, D.; Carmeliet, J. A dynamic pore network model for imbibition simulation considering corner film flow. *Water Resour. Res.* **2022**, 5*8*, e2022WR032332.

29. Afsaneh, H.; Mohammadi, R. Microfluidic platforms for the manipulation of cells and particles. *Talanta* **2022**, 5, 100092.

30. Deng, B.; Wang, H.; Tan, Z.; Quan, Y. Microfluidic cell trapping for single-cell analysis. *Micromachines* **2019**, 10, 409.

31. Deng, Y.; Guo, Y.; Xu, B. Recent Development of Microfluidic Technology for Cell Trapping in Single Cell Analysis: A Review. *Processes* **2020**, 8, 1253.

32. Li, C.; Warrick, J. W.; Li, J.; Geller, S. H.; Trantow, V. G.; Mcclean, M. N.; Beebe, D. J. Under oil open-channel microfluidics empowered by exclusive liquid repellency. *Sci. Adv.* **2020**, 6(16), 9919.

33. Li, Y. F.; Xia, G. D.; Ma, D. D.; Yang, J. L.; Li, W. Experimental investigation of flow boiling characteristics in microchannel with triangular cavities and rectangular fins. *Int. J. Heat Mass Transf.* **2020**, 148, 119036.

34. Rajalingam, A.; Chakraborty, S. Estimation of the thermohydraulic performance of a microchannel heat sink with gradual and sudden variation of the flow passage. *Int. J. Heat Mass Transf.* **2022**, 190, 122776.

35. Tang, J.; Yu, Y.; Hu, X.; Mo, X.; Zhou, W.; Dai, X.; Shan, L.; Yu, D. Study on the characteristics of the capillary wetting and flow in open rectangular microgrooves heat sink. *Appl. Therm. Eng.* **2018**, 143, 90–99.

36. Berthier, J.; Brakke, K.; Berthier, E. A general condition for spontaneous capillary flow in uniform cross-section microchannels. *Microfluid.* **2014**, 16, 779-785.

37. Berthier, J.; Gosselin, D.; Pham, A.; Boizot, F.; Delapierre, G.; Belgacem, N.; Chaussy, D. Spontaneous capillary flows in piecewise varying cross section microchannels. *Sens. Actuators B Chem.* **2016**, 223, 868-877.

38. Berthier, J.; Brakke, K. A.; Gosselin, D.; Navarro, F.; Belgacem, N.; Chaussy, D.; Berthier, E. On the halt of spontaneous capillary flows in diverging open channels. *Med. Eng. Phys.* **2017**, 48, 75-80.

39. Chen, J. M.; Chen, C. Y.; Liu, C. H. Pressure Barrier in an Axisymmetric Capillary Microchannel with Sudden Expansion. *Jpn. J. Appl. Phys.* **2008**, 47, 1683.

40. Ferrás, L. L.; Afonso, A. M.; Alves, M. A.; Nóbrega, J. M.; Pinho, F. T. Newtonian
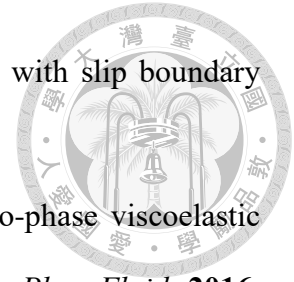
and viscoelastic fluid flows through an abrupt 1:4 expansion with slip boundary conditions. *Phys. Fluids* **2020**, 32, 043103.

41. Izbassarov, D.; Muradoglu, M. A computational study of two-phase viscoelastic systems in a capillary tube with a sudden contraction/expansion. *Phys. Fluids* **2016**, 28, 012110.

42. Luo, Z. Y.; Bai, B. F. Solute release from an elastic capsule flowing through a microfluidic channel constriction. *Phys. Fluids* **2019**, 31, 121902.

43. Pavuluri, S.; Maes, J.; Yang, J.; Regaieg, M.; Moncorge, A.; Doster, F. Towards pore network modelling of spontaneous imbibition: contact angle dependent invasion patterns and the occurrence of dynamic capillary barriers. *Comput. Geosci.* **2020**, 24, 951-969.

44. Lee, J. J.; Berthier, J.; Brakke, K. A.; Dostie, A. M.; Theberge, A. B.; Berthier, E. Droplet Behavior in Open Biphasic Microfluidics. *Langmuir* **2018**, 34, 5358-5366.

45. Chu, K.-C.; Tsao, H.-K.; Sheng, Y.-J. Penetration dynamics through nanometer-scale hydrophilic capillaries: Beyond Washburn's equation and extended menisci. *J. Colloid Interface Sci.* **2019**, 538, 340-348.

46. Warren, P. B. Vapor-liquid coexistence in many-body dissipative particle dynamics. *Phys. Rev. E* **2003**, 68, 066702.

47. Zhao, J.; Chen, S.; Zhang, K. A review of many-body dissipative particle dynamics (MDPD): Theoretical models and its applications. *Phys. Fluids* **2021**, 33, 112002.

48. Chu, K.-C.; Tsao, H.-K.; Sheng, Y.-J. Spontaneous spreading of nanodroplets on partially wetting surfaces with continuous grooves: Synergy of imbibition and capillary condensation. *J. Mol. Liq.* **2021**, 339, 117270.

49. He, G.-Y.; Tsao, H.-K.; Sheng, Y.-J. Wicking dynamics into two-rail open channel with periodical branches. *Phys. Fluids* **2022**, 34, 102004.

50. Chen, Y.-F.; Xiao, S.; Chen, H.-Y.; Sheng Y.-J.; Tsao, H.-K. Enhancing rectification of a nano-swimmer system by multi-layered asymmetric barriers. *Nanoscale* **2015**, 7, 16451–16459.

51. Xu, J.; Yang, C.; Tsao, H.-K.; Sheng, Y.-J. Apparent hydrodynamic slip induced by density inhomogeneities at fluid–solid interfaces. *Soft Matter* **2015**, 11(35), 6916-6920.

52. Wang, S.; Zhang, X.; Ma, C.; Yan, S.; Inglis, D.; Feng, S. A Review of Capillary Pressure Control Valves in Microfluidics. *Biosensors* **2021**, 11, 405.

53. Jokinen, V.; Franssila, S. Capillarity in microfluidic channels with hydrophilic and hydrophobic walls. *Microfluid.* **2008**, 5, 443-448.